Letter

Superconductivity of repulsive spinless fermions with sublattice potentials

Yuchi He [1,*] Kang Yang,[2,†] Jonas B. Profe [1,‡] Emil J. Bergholtz [2,§] and Dante M. Kennes[1,3,¶]

[1]*Institut für Theorie der Statistischen Physik, RWTH Aachen University and JARA—Fundamentals of Future Information Technology, 52056 Aachen, Germany*

[2]*Department of Physics, Stockholm University, AlbaNova University Center, 106 91 Stockholm, Sweden*

[3]*Max Planck Institute for the Structure and Dynamics of Matter, Center for Free Electron Laser Science, 22761 Hamburg, Germany*

(Received 13 August 2022; revised 6 January 2023; accepted 10 January 2023; published 26 January 2023)

We explore unconventional superconductivity of repulsive spinless fermions on square and honeycomb lattices with staggered sublattice potentials. The two lattices can exhibit staggered d-wave and f-wave pairing, respectively, at low doping stemming from an effective two-valley band structure. At higher doping, in particular, the square lattice displays a much richer phase diagram including topological $p+ip$ superconductivity which is induced by a qualitatively different mechanism compared to the d-wave pairing. We illuminate this from several complementary perspectives: We analytically perform sublattice projection to analyze the effective continuum low-energy description and we numerically calculate the binding energies for pair and larger bound states for few-body doping near half filling. Furthermore, for finite doping, we present phase diagrams based on extensive functional renormalization group and and density matrix renormalization group calculations.

DOI: 10.1103/PhysRevResearch.5.L012009

Introduction. There have been substantial efforts [1–4] to understand superconductivity mechanisms beyond the conventional phonon-mediated [5] electron-electron attraction. In one category of mechanisms, bare repulsive electron-electron interaction becomes effectively attractive due to virtual processes after projections to the sublattice or bands [6–8]. Recently, exact results for an effective attraction have been obtained for fermionic honeycomb lattice models with a large staggered sublattice potential [9–11]. This mechanism can be essentially captured by a minimal model of spinless fermions [9], of which the low-energy physics projected to one sublattice shows effective attraction. Such a mechanism has been argued to be relevant for triplet pairing in materials [10,12–14].

In this Letter we study the pairing of spinless fermions on the square lattice in addition to the honeycomb lattice model studied in Ref. [9]. Studying a different lattice can shed light on the relevance of the proposed pairing mechanism to layered materials, in which different lattice structures can be realized [15]. Considering a different lattice contributes to further understanding the ingredients of the sublattice projection mechanism for superconductivity—and, as we show, reveals qualitatively different possibilities. The effective theory from a sublattice projection depends on the coordination number of the lattices; lattice symmetry is crucial for the realization of different types of unconventional superconductivity [16–20].

The overall result is summarized in Fig. 1. The quantum phases are inferred through infinite density matrix renormalization group (DMRG) [21,22] data for strong coupling combined with functional renormalization group (FRG) [23] data at weak coupling. Superconducting phases are found in a wide range of interaction parameters in the honeycomb model while its regime is limited to smaller interactions for the square model. Compared to a previous study [9], a significant difference is that there are two superconducting phases on the square lattice, the staggered d-wave and the $p+ip$ topological phases, in contrast to the sole f-wave pairing on the honeycomb lattice. The d-wave pairing on the square lattice shares the same origin as the f-wave pairing on the honeycomb lattice in the sense of inter-valley pairing. The Cooper pair arises from an inter-valley attraction revealed by sublattice projection. This requires a next-nearest-neighbor hopping t' to realize a two-valley band structure for the square lattice. Upon increasing doping, we observe a transition from staggered d to a topological $p+ip$ [24] superconductor. With zero momentum, $p+ip$ no longer results from the intervalley attraction. It does not require the next-nearest-neighbor hopping. Moreover, at stronger interactions, we find evidence for a transition from superconductivity to inhomogeneous states.

Model and low-energy description. We use the square lattice [Fig. 1(ai)] as an example while the honeycomb model [Fig. 1(aii)] can be found in Ref. [9] with the same form of Hamiltonian. The Hamiltonian is taken as

$$H = \sum_{\langle i,j\rangle}[-(tc_i^\dagger c_j + \text{H.c.}) + Vn_in_j] - \sum_{\ll i,j\gg}(t'c_i^\dagger c_j + \text{H.c.}) + \sum_{i\in B} Dn_i, \quad (1)$$

*yuchi.he@rwth-aachen.de
†kang.yang@fu-berlin.de
‡jonas.hauck@rwth-aachen.de
§emil.bergholtz@fysik.su.se
¶dante.kennes@mpsd.mpg.de

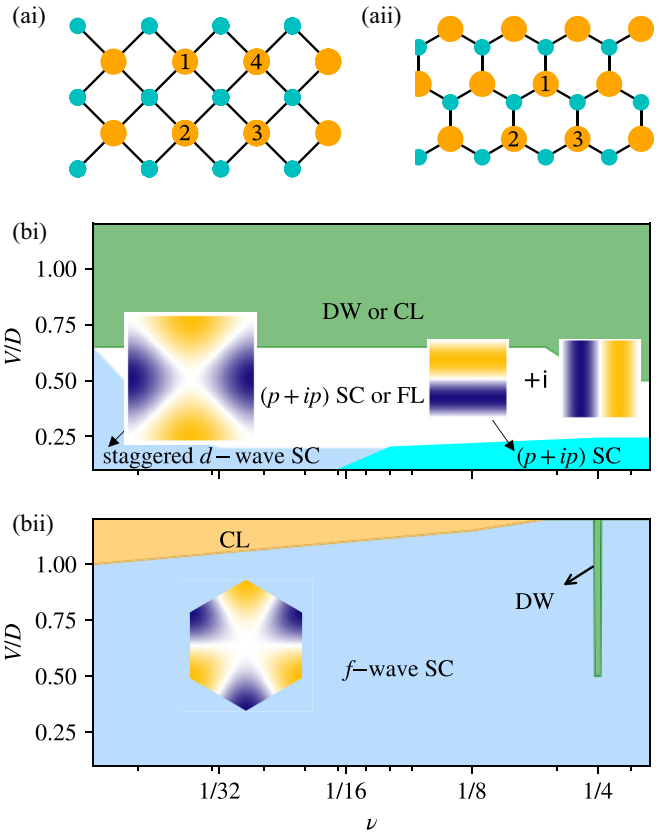

FIG. 1. Lattice structure and schematic phase diagrams. (a) Lattice structure for (ai) square and (aii) honeycomb lattices; sublattices are marked in orange and cyan. (b) Phase diagram for (bi) the square lattice with $t' = \lambda_0$ and (bii) the honeycomb lattice with $t' = 0$, inferred from FRG (weak coupling) and DMRG (strong coupling). For superconducting phases, we plot the momentum dependence of the susceptibility from FRG. For the $p + ip$ SC phase, a degenerate pair of dominant eigenvectors is found in FRG, and a mean-field analysis indicates the linear combination $p + ip$ is favored. Here DW denotes the density-wave phase, CL denotes a phase separation via the collapse of electrons on the B sublattice, and FL denotes Fermi liquids. For the uncertainty in the DMRG data interpretation, see the discussion in the text.

where c_i, ($c_i^\dagger$) is the fermionic annihilation (creation) operator on site i, and $n_i = c_i^\dagger c_i$. The symbols $\langle i, j\rangle$ and $\ll i, j \gg$ denote nearest neighbors and next-nearest neighbors, respectively. We limit our attention to repulsive interaction $V > 0$ and sublattice potential $D \gg |t| > 0$ on the sublattice B. At half filling and large D, the ground state is expected to have the A sublattice fully filled and the B sublattice unfilled. When $t' = 0$, the Hamiltonian exhibits an explicit symmetry of particle-hole transformation $c_A^\dagger \to c_A$ and $c_B^\dagger \to -c_B$ combined with spatial inversion that interchanges the sublattices. When $t' \neq 0$, the combined particle-hole transformation equivalently changes the sign of t'. In this work we will only introduce $t' \neq 0$ on the square lattice while $t' = 0$ on the honeycomb lattice, which is motivated by the discussion below. We focus on electron doping the system near half filling, where the low-energy physics is controlled by those extra electrons on the B lattice. The effective model is derived by

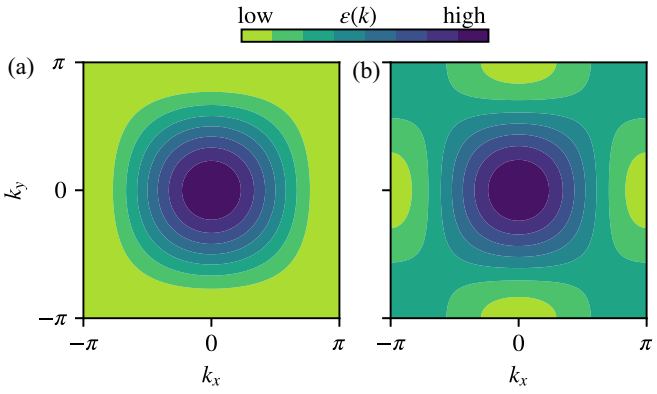

FIG. 2. Band structures of the square lattice's effective model's kinetic part at (a) $t' = 0$ and (b) $t' = \lambda_0$. The right band structure has two valleys at $(0, \pm\pi)$ and $(\pm\pi, 0)$, respectively. The two-valley structure is absent for $t' = 0$ [in (a)].

a Schrieffer-Wolff transformation [25,26] (for details see the Supplemental Material [27]). Up to the second order of t, this effective Hamiltonian contains terms of hopping, correlated hopping, and interactions: $H_{\text{eff}} = H_{\text{hopping}} + H_{\text{ch}} + H_U$.

Different parts of the Hamiltonian are introduced as follows (for details of the coefficients see [27]): H_{hopping} contains nearest-neighbor $\langle ij\rangle$ and next-nearest-neighbor $\ll ij \gg$ terms for the sublattice B,

$$H_{\text{hopping}} = \left[\sum_{\langle ij\rangle} t_B c_{i,B}^\dagger c_{j,B} + \sum_{\ll ij\gg} t_B' c_{i,B}^\dagger c_{j,B}\right] + \text{H.c.}, \quad (2)$$

where $t_B = 2\lambda_0 - t'$ and $t_B' = \lambda_0$, with $\lambda_0 = t^2/(D + 2V)$. For most of our calculations, we will either fix $t' = 0$ or $t' = \lambda_0$.

The correlated hopping also includes two terms

$$H_{\text{ch}} = \sum_{ijk\in\square} \lambda_1 c_{i,B}^\dagger c_{j,B} n_{k,B} + \sum_{ijkl\in\square} \frac{\lambda_2}{2} c_{i,B}^\dagger c_{j,B} n_{k,B} n_{l,B}. \quad (3)$$

The combinations ijk and $ijkl$ are summed over all possible ordered vertices of plaquettes in the B sublattice, e.g., 1, 2, 3, and 4 in Fig. 1(ai). Finally, there are two-, three-, and four-body density interactions

$$H_U = \sum_{\langle ij\rangle} 2U_2 n_{i,B} n_{j,B} + \sum_{\langle\ll ij\gg} U_2 n_{i,B} n_{j,B} + \sum_{[ijk]\in\square} U_3 n_{i,B} n_{j,B} n_{k,B} + \sum_{[ijkl]\in\square} U_4 n_{i,B} n_{j,B} n_{k,B} n_{l,B}. \quad (4)$$

The combinations $[ijk]$ and $[ijkl]$ are summed over all possible unordered vertices of plaquettes in sublattice B. The four-body interaction U_4 remains repulsive in the full parameter region, while other interaction terms turn from repulsion to attraction when increasing across $V/D = 1$.

The dispersion of the kinetic part H_{hopping} depends on the next-nearest-neighbor hopping t'. At $t' = 0$ [shown in Fig. 2(a)], the band minimum is located along the boundary of the Brillouin zone. The Fermi surface is connected and has an approximate rotation symmetry. By tuning t' such that $|t_B'/t_B| > 0.5$, two band minima appear at $(0, \pm\pi)$ and

$(\pm\pi, 0)$, respectively, where the unit of the wave vectors is $1/a$. The low-energy physics is then controlled by these two valleys which are interchanged under a $\pi/2$ rotation. When tuning to higher doping, the Fermi surface includes the Van Hove singularities. They are located at $(q, \pm q)$ with $q = \pm \arccos(-t_B/2t'_B)$. The two-valley low-energy physics is replaced by the one exhibiting new instabilities driven by the higher density of states. We remark that introducing t' on the honeycomb lattice only brings an overall factor to the band dispersion.

Two-valley continuum theory of the square lattice model. To construct the continuum theory in the case with two valleys, the degrees of freedom for doped electrons can be decomposed into two valleys: $c_j = \sum_\sigma a \exp[i\mathbf{K}_\sigma \cdot \mathbf{r}_j]\psi_\sigma(\mathbf{r}_j)$ with $\mathbf{K}_+ = (0, \pi)$ and $\mathbf{K}_- = (\pi, 0)$, where the fields $\psi_\sigma(\mathbf{r})$ vary slowly at the scale of a, the minimal distance between two B-sublattice sites.

At low doping, we ignore the three- and four-body interactions in H_U. The continuum Hamiltonian includes a kinetic part with anisotropic masses $\sum_\sigma \psi^\dagger_\sigma \partial_x^2 \psi_\sigma/2m^{xx}_\sigma + \psi^\dagger_\sigma \partial_y^2 \psi_\sigma/2m^{yy}_\sigma$ at two valleys and a two-body interaction term. There are two contributions to the two-body interaction in the continuum limit, the correlated hopping terms in Eq. (3) and the two-body repulsion terms Eq. (4). In the long-wavelength limit, the interaction can be written as

$$\int d^2\mathbf{r}\, g\psi^\dagger_+(\mathbf{r})\psi_+(\mathbf{r})\psi^\dagger_-(\mathbf{r})\psi_-(\mathbf{r}), \tag{5}$$

where $g = (16U_2 - 32\lambda_1)a^2 = 16a^2[-4t^2/(D+3V) + 8t^2(D+2V) - 4t^2/(D+3V)] < 0$, indicating two-particle ground states are always intervalley bound states. A possible low-doping superconducting (SC) state arises from a condensate of intervalley pairing $\langle\psi_+(\mathbf{r})\psi_-(\mathbf{r})\rangle \neq 0$. In terms of microscopic fields, we find a total momentum (π, π), $d_{x^2-y^2}$ pairing with an order parameter $\langle c_i c_j\rangle = [(-1)^{i_x+j_y} - (-1)^{i_y+j_x}]\Delta(i-j)$, where Δ is odd under a $\pi/2$ rotation. While the pair has nonzero total momentum, the above reasoning for the pairing is the same as that for f-wave SC of low-doping honeycomb model [11]. For finite doping, realizing pairing with (π, π) center-of-mass momentum is frustrated by the shape of the Fermi surfaces. This could lead to a transition to incommensurate (not observed) or other SC phases. Inferring the possible SC at finite doping from the bare Hamiltonian of the projected model is no longer simple. The complication comes from the interactions projected on the Fermi surface. Nevertheless, we can show that for the intravalley interaction, the correlated hopping in the projected model can induce bare attractive interaction term between pairs of fermion modes on the Fermi surface with zero net momentum, for details see the Supplemental Material [27]. Thereby the possibility of intravalley pairing, likely p-wave pairing, is suggested. We will later discuss the role of Van Hove singularity for SC, which is independent of the role of projected interactions.

Binding energies for few-particle doping. Next we show our numerical results of pair and larger bound states formation in the dilute doping limit. Binding energies can be deduced from the difference between one-particle doping energy and energy per particle of n-particle doping; the data for the effective model ($D/t = \infty$) are plotted in Fig. 3. (Our data for $D/t = 5, 10$ can be found in Ref. [27].) From the data, we can infer that at $D/t = \infty$, there can be a stable dilute pairing phase for the honeycomb lattice with $V/D \lessapprox 1$. The pairing phase is not favored for the square lattice with $t' = 0$, but it can exist with $t' > 0$. For $t' = \lambda_0$, the condition for pairing phase is $V/D \lessapprox 0.6$.

We also determine the momenta of the few-particle ground states. The momentum of a pair for the square lattice with $t' = \lambda_0$ and the honeycomb lattice, are respectively (π, π) and (0,0). Recall that two valleys of the honeycomb lattice are located at $\pm\mathbf{K}$ (standard notation [28]), and those of the square lattice model are located at $(\pi, 0)$ or $(0, \pi)$. This along with finite pair binding energy results indicates an inter-valley pairing mechanism and explains the absence of it in the case of $t' = 0$ with the absence of valleys. The two-valley structure allows stable pairing, for which a sufficient attraction between fermions in different valleys exists but no attractions sufficient for larger bound states. The latter condition can be usually met with weak coupling as the intravalley coupling is less relevant in the dilute doping limit.

Numerical study of the quantum phases at finite doping. The above few-body and continuum theory results provide an indication of superconductivity at low doping and its instability for large interactions. In the following, we apply DMRG and FRG to infer the quantum phases of the full models with $D = 10$ and $t' = \lambda_0$ (square) and $t' = 0$ (honeycomb) at finite fermion doping from weak to strong coupling (details see the Supplemental Material [27]); the results are summarized in Fig. 1. The $d_{x^2-y^2}$- and f-wave superconductivity of square and honeycomb lattice expected at dilute doping are observed by both methods. Upon increasing doping of the square lattice by approximately 0.1, our FRG calculation indicates a $p + ip$ superconducting phase. In the honeycomb lattice model, the f-wave superconductivity persists for higher doping, corroborating the main claim of Refs. [9,11]; but our DMRG data suggest the absence of superconductivity at the Van Hove singularity $\nu = \frac{1}{4}$, in contrast to Refs. [9,11]. Recall that near the Van Hove singularity the two-valley picture breaks down.

In the weak coupling regime ($V/D \lessapprox 0.3$), we perform FRG calculations [23,29] at the one-loop level. We only include the static self-energy and the static two-particle interaction. More particle processes are only included as virtual processes in the two-particle vertex. The inclusion of the static self-energy has been shown to cover already the relevant physics in one-dimensional (1D) systems [30] and can be argued to cover the relevant physics more generally by power counting arguments [23]. The static self-energy incorporates possible further increases of the band gap and deformations of the Fermi surface. For our simulations, we use the unified truncated unity (dubbed TU^2) approach [31] merging real and momentum space, which has been demonstrated to fulfill in the FRG equivalence class [32]. We distinguish different phases in our FRG simulations by inspecting the eigenvectors corresponding to the largest eigenvalue of each diagrammatic channel. Each of these channels corresponds to a different type of instability and the symmetry of the eigenvector gives the symmetry of the ordering. The Fourier transformation of these eigenvectors at the B sublattice are visualized as insets in Fig. 1. In the strong-coupling regime ($V/D \gtrapprox 0.5$),

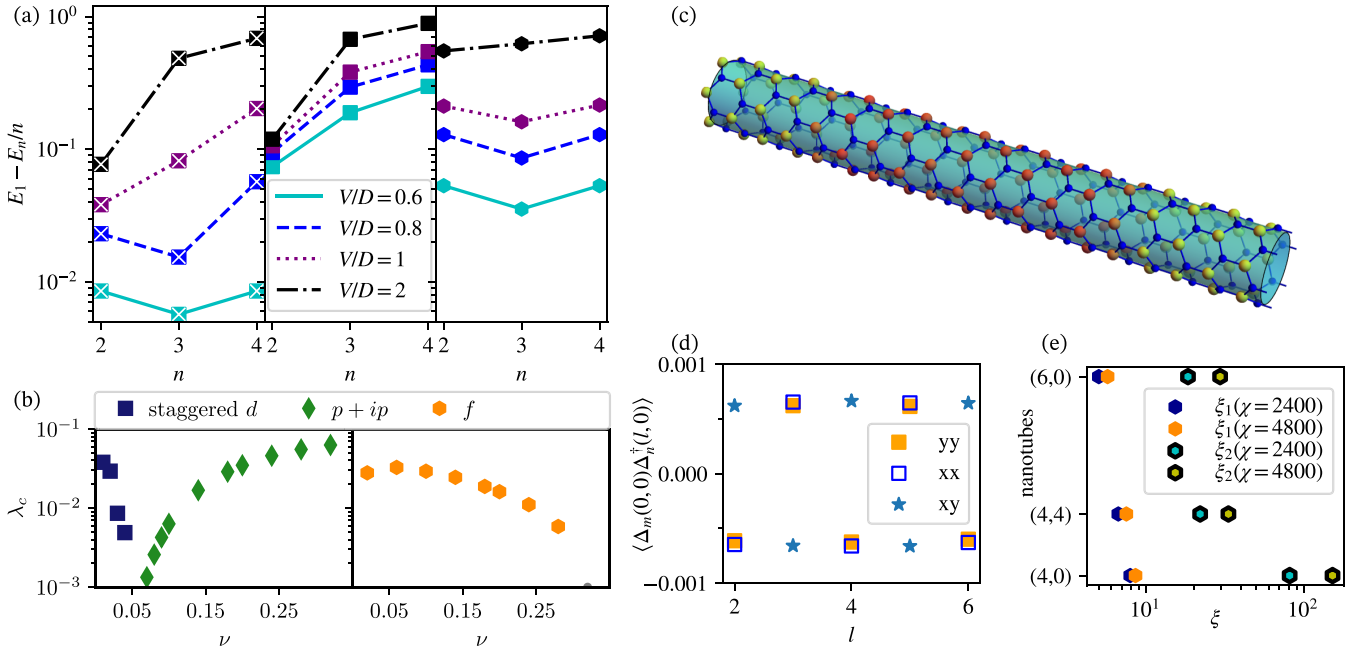

FIG. 3. Results from exact diagonalization (ED) of the effective model for few-particle doping, with FRG and DMRG of the full model for finite doping. (a) Energy per particle of the n-particle ground states; the unit is t^2/D. Calculations are performed for the effective models using ED with finite-size extrapolation. From left to right are the square lattice model with $t' = \lambda_0$ and the honeycomb lattice $t' = 0$. Finite $E_1 - E_2/2$ indicates the existence of two-particle bound states. Some paired phase near the dilute limit is indicated by that the energy per particle $E_1 - E_n/n$ is a constant for every positive even n and larger than the values for odd n. On the other hand, if there is some n, with $E_1 - E_n/n$ greater than $E_1 - E_2/2$, larger bound states are favored. (b) FRG predicted phases and energy scales λ_c in units of t^2/D. Shown on the left is the square lattice model with $t' = \lambda_0$ and on the right is the honeycomb lattice. We choose $V = 2t$ as the interaction. (c) Cylinder geometry [(6,0) honeycomb nanotube] and a density plot of an inhomogeneous density profile, indicating phase separation. The densities on sublattice B are represented by colors, with green for low density and red for higher density. The parameters for the density plot are $\frac{1}{8}$ doping, $D = 10$, $V = 15$, and unit cell size 32; only part of the unit cell is plotted. (d) Pair correlation functions for square lattice at $\frac{1}{64}$ doping, $V = 6$, $D = 10$, and a tangential direction size of eight unit cells. For definitions of the pair operators see the text; the subscripts m and n can be x and y. (e) Correlation length evidence for pairing on the infinite cylinder geometry of a honeycomb lattice. The indices for nanotubes are standard notation for their sizes and shapes. The ξ_1 (ξ_2) is the single-particle (pair) correlation length. For a larger bond dimension χ used in the iDMRG algorithm, a tighter lower bound of ξ is obtained. Here a smaller $\xi_2(\chi)$ for a larger nanotube is an artifact of the underestimation becoming more severe for larger systems for fixed χ. The other parameters are $\frac{1}{8}$ doping and $D = V = 5$.

we use DMRG [21,22] to obtain ground states on infinite cylinder geometries [33]. We consider cylinders with up to eight sites along the circumference. The counterpart of 2D superconductivity on the cylinder cannot retain long-range order because of the Mermin-Wagner theorem. However, the pair correlation is expected to be dominant over single-particle correlation. In most common cases, the single-particle excitation of a quasi-1D system is fully gapped (see, e.g., Ref. [34]); the single-particle correlation length ξ_1 is finite, while the pair correlation length ξ_2 can diverge. Thus, observation of estimated $\xi_2 \gg \xi_1$ serves as evidence for such pairing. The DMRG estimation [35–37] usually sets lower bounds for correlation lengths, which become tighter with an increasing number of variational parameters characterized by bond dimension χ [37].

For the square lattice, we find the predicted $d_{x^2-y^2}$-wave superconductor at low doping within our FRG simulations with $t' = \lambda_0$. However, the critical energy scale drops rapidly upon increasing doping and at higher doping ($\nu \approx 0.1$) we observe a transition to a $p_x + ip_y$ topological superconductor with Chern number [38] $\mathcal{C} = 2$. The low-doping phase is expected from the above bare interaction analysis. Besides the bare interaction terms revealed above, we speculate a density-fluctuation-mediated mechanism [39] can be crucial for stabilizing the higher-doping SC. One observation is a clear increase of SC energy scale at higher doping closer to the density state maxima [Fig. 3(b)]. The transition between the phases seems to be driven by a change of weight within the particle-particle loop, whereupon doping the $d_{x^2-y^2}$ eigenvector will be increasingly suppressed while the p_x/p_y pair will increase in strength. At stronger interactions ($V/D \approx 0.25$) our FRG breaks down, manifested as a linear ramp-up of the density-density interaction. This ramp-up marks the breakdown of the perturbative regime and hence FRG cannot be used to examine the phases. We additionally study the case $t' = 0$ for which the two valleys are absent, the ramp-up problem exists at low doping even for weak interaction, and a $\mathcal{C} = 1$ $p + ip$ is observed for some higher doping [27]. From the DMRG data ($V/D \gtrapprox 0.5$ and $t' = \lambda_0$), a finite single-particle correlation length ξ_1 is only consistently found in low doping, approximately $\frac{1}{64}$, and intermediate interaction; in this case, the pair correlation shows a dominant oscilla-

tory part, supporting the staggered $d_{x^2-y^2}$ pairing [Fig. 3(d)]. We study the geometry with the axial direction along the shortest lattice unit vector [e.g., that connecting nodes 1 and 2 in Fig. 1(ai)]. We consider two-point correlations between $\Delta_x(i_x, i_y) = c_{i_x,i_y} c_{i_x+1,i_y}$, $\Delta_y(i_x, i_y) = c_{i_x,i_y} c_{i_x,i_y+1}$ and their Hermitian conjugation. Only the sites on sublattice B are considered. We observe that the signs of $\langle \Delta_x(0,0)\Delta_x^\dagger(l,0)\rangle$ and $\langle \Delta_y(0,0)\Delta_y^\dagger(l,0)\rangle$ oscillate in l; we also observe that the sign of $\langle \Delta_x(0,0)\Delta_y^\dagger(l,0)\rangle$ is opposite to the previous two for a given l. For higher doping, no evidence of convergent ξ_1 is found and no evidence for time-reversal symmetry breaking is found for the larger bond dimensions implemented. While these can be features of a quasi-1-D analog of a Fermi liquid (FL), topological $p+ip$ pairing cannot be excluded. The particle-number-conserved 1D analog of the topological p-wave state has been suggested to be adiabatically connected to an FL [40]; a deeper understanding of the quasi-1D analog of $p+ip$ is needed to better interpret the data for the $p+ip$ SC or FL region of Fig. 1(b i). The region for large V/D denoted by DW in Fig. 1 is characterized by inhomogeneous densities within the implemented bond dimensions. The 2D phases are speculated to be charge density waves at sufficient commensurate doping; other doping could be Fermi liquids or phases separated by Maxwell construction. The density-wave patterns are difficult to determine as they may only fit on larger cylinders than those studied.

For the honeycomb lattice, we observe f-wave superconductivity in FRG for a broad range of doping, which exceeds Van Hove doping $\frac{1}{4}$. The range is slightly smaller than the random-phase approximation result Ref. [11]. Similar to the square lattice, there is also a ramp-up refraining FRG prediction at stronger coupling. Our DMRG for stronger coupling shows a broad range for pairing with a single-particle gap. This is observed for all geometries we studied [see, e.g., Fig. 3(e)], including the zigzag and armchair nanotube geometries, denoted by $(n, 0)$ and (n, n) (standard notation [33]), respectively, where n characterizes the circumference. However, right at the Van Hove doping $\nu = \frac{1}{4}$, most cylinder setups, including the largest, point to insulating states [27]. This feature indicates a possible mechanism of density-fluctuation-induced SC which can accompany a density-wave phase at a commensurate filling [18]. This independent mechanism for f-wave SC provides an explanation why the phase extends to higher doping compared to the previous estimation of the bare interaction [11]. However, the SC energy scale is not largely enhanced closer to the density of states maxima [Fig. 3(b)], in contrast to the square lattice. This point is further supported by the high doping state still being an f-wave superconductor [18], such that no competition between the mechanisms is realized. The CL indicates the collapse of fermions leaving part of the system with vanishing occupancy on the B sublattice; collapses are usually observed for models with strong attractive interactions [19,41,42]. The observation is that the fermions on lattice B always concentrate on part of the unit cell [see Fig. 3(c)] when increasing iMPS unit cell size.

Discussion. We examined fermion pairing driven by repulsive interaction and a strong sublattice potential for square lattices and honeycomb lattices. The honeycomb lattice is confirmed to show f-wave pairing, which can be interpreted as intervalley pairing. The square lattice's counterpart of intervalley pairing is found to give a low-doping d-wave superconductivity with (π, π) total momentum. Upon increasing doping, a $p+ip$ topological superconductivity is found. Because of the role and existence condition of valleys, the square lattice model with next-nearest-neighbor hopping can exhibit an asymmetry for electron and hole doping. As an outlook, one may also include spin degrees of freedom [10,43] and more types of interactions and hoppings, which serve as extensions of ionic Hubbard models [44–48]. This may have implications for real materials and provide the possibility of the sought-after $p+ip$ superconductivity with topological order.

Acknowledgments. We thank Johan Carlström, Biao Huang, Ciarán Hickey, Dominik Kiese, Lennart Klebl, Lukas Weber, Stefan Wessel, and Fan Yang for discussions. The QuSpin [49] and TeNPy [50] packages were used for the numerical studies. The authors gratefully acknowledge the computing time granted by the Max Planck Computing and Data Facility. The authors gratefully acknowledge the computing time granted by the JARA Vergabegremium and provided on the JARA Partition part of the supercomputer JURECA [51] at Forschungszentrum Jülich. Y.H., J.B.P., and D.M.K. were supported by the Deutsche Forschungsgemeinschaft (German Research Foundation) under Grant No. RTG 1995, within the Priority Program SPP 2244 "2DMP" and under Germany's Excellence Strategy–Cluster of Excellence Matter and Light for Quantum Computing (ML4Q) Grant No. EXC 2004/1-390534769. K.Y. and E.J.B. were supported by the Swedish Research Council (Grant No. 2018-00313) and the Wallenberg Academy Fellows program of the Knut and Alice Wallenberg Foundation (Grant No. 2018.0460).

[1] W. Kohn and J. M. Luttinger, New Mechanism for Superconductivity, Phys. Rev. Lett. **15**, 524 (1965).
[2] P. A. Lee, N. Nagaosa, and X.-G. Wen, Doping a Mott insulator: Physics of high-temperature superconductivity, Rev. Mod. Phys. **78**, 17 (2006).
[3] M. R. Norman, The challenge of unconventional superconductivity, Science **332**, 196 (2011).
[4] G. R. Stewart, Unconventional superconductivity, Adv. Phys. **66**, 75 (2017).
[5] J. Bardeen, L. N. Cooper, and J. R. Schrieffer, Theory of superconductivity, Phys. Rev. **108**, 1175 (1957).
[6] W. A. Little, Possibility of synthesizing an organic superconductor, Phys. Rev. **134**, A1416 (1964).
[7] X. Chen, S. Maiti, A. Linscheid, and P. J. Hirschfeld, Electron pairing in the presence of incipient bands in iron-based superconductors, Phys. Rev. B **92**, 224514 (2015).
[8] Z. Dong and L. Levitov, Activating superconductivity in a repulsive system by high-energy degrees of freedom, arXiv:2103.08767.
[9] V. Crépel and L. Fu, New mechanism and exact theory of superconductivity from strong repulsive interaction, Sci. Adv. **7**, eabh2233 (2021).

[10] V. Crépel and L. Fu, Spin-triplet superconductivity from excitonic effect in doped insulators, Proc. Natl. Acad. Sci. USA **119**, e2117735119 (2022).

[11] V. Crépel, T. Cea, L. Fu, and F. Guinea, Unconventional superconductivity due to interband polarization, Phys. Rev. B **105**, 094506 (2022).

[12] Y. Nakagawa, Y. Kasahara, T. Nomoto, R. Arita, T. Nojima, and Y. Iwasa, Gate-controlled BCS-BEC crossover in a two-dimensional superconductor, Science **372**, 190 (2021).

[13] V. Fatemi, S. Wu, Y. Cao, L. Bretheau, Q. D. Gibson, K. Watanabe, T. Taniguchi, R. J. Cava, and P. Jarillo-Herrero, Electrically tunable low-density superconductivity in a monolayer topological insulator, Science **362**, 926 (2018).

[14] E. Sajadi, T. Palomaki, Z. Fei, W. Zhao, P. Bement, C. Olsen, S. Luescher, X. Xu, J. A. Folk, and D. H. Cobden, Gate-induced superconductivity in a monolayer topological insulator, Science **362**, 922 (2018).

[15] S. Zhang, M. Tanaka, E. Watanabe, H. Zhu, K. Inumaru, and S. Yamanaka, Superconductivity of alkali metal intercalated TiNBr with α-type nitride layers, Supercond. Sci. Technol. **26**, 122001 (2013).

[16] M. Sigrist and K. Ueda, Phenomenological theory of unconventional superconductivity, Rev. Mod. Phys. **63**, 239 (1991).

[17] M. Cheng, K. Sun, V. Galitski, and S. Das Sarma, Stable topological superconductivity in a family of two-dimensional fermion models, Phys. Rev. B **81**, 024504 (2010).

[18] S. Hesselmann, D. D. Scherer, M. M. Scherer, and S. Wessel, Bond-ordered states and f-wave pairing of spinless fermions on the honeycomb lattice, Phys. Rev. B **98**, 045142 (2018).

[19] K.-H. Ma and N.-H. Tong, Interacting spinless fermions on the square lattice: Charge order, phase separation, and superconductivity, Phys. Rev. B **104**, 155116 (2021).

[20] N. Gneist, D. Kiese, R. Henkel, R. Thomale, L. Classen, and M. M. Scherer, Functional renormalization of spinless triangular-lattice fermions: N-patch vs. truncated-unity scheme, Europ. Phys. J. B **95**, 157 (2022).

[21] S. R. White, Density Matrix Formulation for Quantum Renormalization Groups, Phys. Rev. Lett. **69**, 2863 (1992).

[22] I. P. McCulloch, Infinite size density matrix renormalization group, revisited, arXiv:0804.2509.

[23] W. Metzner, M. Salmhofer, C. Honerkamp, V. Meden, and K. Schönhammer, Functional renormalization group approach to correlated fermion systems, Rev. Mod. Phys. **84**, 299 (2012).

[24] N. Read and D. Green, Paired states of fermions in two dimensions with breaking of parity and time-reversal symmetries and the fractional quantum Hall effect, Phys. Rev. B **61**, 10267 (2000).

[25] A. H. MacDonald, S. M. Girvin, and D. Yoshioka, $\frac{t}{U}$ expansion for the Hubbard model, Phys. Rev. B **37**, 9753 (1988).

[26] A. L. Chernyshev, D. Galanakis, P. Phillips, A. V. Rozhkov, and A.-M. S. Tremblay, Higher order corrections to effective low-energy theories for strongly correlated electron systems, Phys. Rev. B **70**, 235111 (2004).

[27] See Supplemental Material at http://link.aps.org/supplemental/10.1103/PhysRevResearch.5.L012009 for details.

[28] A. H. Castro Neto, F. Guinea, N. M. R. Peres, K. S. Novoselov, and A. K. Geim, The electronic properties of graphene, Rev. Mod. Phys. **81**, 109 (2009).

[29] N. Dupuis, L. Canet, A. Eichhorn, W. Metzner, J. Pawlowski, M. Tissier, and N. Wschebor, The nonperturbative functional renormalization group and its applications, Phys. Rep. **910**, 1 (2021).

[30] L. Markhof, B. Sbierski, V. Meden, and C. Karrasch, Detecting phases in one-dimensional many-fermion systems with the functional renormalization group, Phys. Rev. B **97**, 235126 (2018).

[31] J. B. Hauck and D. M. Kennes, TU^{2}FRG: a scalable approach for truncated unity functional renormalization group in generic fermionic models, Eur. Phys. J. B **95**, 60 (2022).

[32] J. Beyer, J. B. Hauck, and L. Klebl, Reference results for the momentum space functional renormalization group, Eur. Phys. J. B **95**, 65 (2022).

[33] S. B. Sinnott and R. Andrews, Carbon nanotubes: Synthesis, properties, and applications, Crit. Rev. Solid State Mater. Sci. **26**, 145 (2001).

[34] C. Peng, Y. Wang, J. Wen, Y. Lee, T. Devereaux, and H.-C. Jiang, Enhanced superconductivity by near-neighbor attraction in the doped Hubbard model, arXiv:2206.03486.

[35] V. Zauner, D. Draxler, L. Vanderstraeten, M. Degroote, J. Haegeman, M. M. Rams, V. Stojevic, N. Schuch, and F. Verstraete, Transfer matrices and excitations with matrix product states, New J. Phys. **17**, 053002 (2015).

[36] Y. He, D. Pekker, and R. S. K. Mong, One-dimensional repulsive Hubbard model with mass imbalance: Orders and filling anomaly, Phys. Rev. B **104**, 195126 (2021).

[37] F. Pollmann, S. Mukerjee, A. M. Turner, and J. E. Moore, Theory of Finite-Entanglement Scaling at One-Dimensional Quantum Critical Points, Phys. Rev. Lett. **102**, 255701 (2009).

[38] T. Fukui, Y. Hatsugai, and H. Suzuki, Chern numbers in discretized Brillouin zone: Efficient method of computing (spin) Hall conductances, J. Phys. Soc. Jpn. **74**, 1674 (2005).

[39] D. J. Scalapino, E. Loh, and J. E. Hirsch, Fermi-surface instabilities and superconducting d-wave pairing, Phys. Rev. B **35**, 6694 (1987).

[40] C. L. Kane, A. Stern, and B. I. Halperin, Pairing in Luttinger Liquids and Quantum Hall States, Phys. Rev. X **7**, 031009 (2017).

[41] Y. He, B. Tian, D. Pekker, and R. S. K. Mong, Emergent mode and bound states in single-component one-dimensional lattice fermionic systems, Phys. Rev. B **100**, 201101(R) (2019).

[42] L. Gotta, L. Mazza, P. Simon, and G. Roux, Pairing in spinless fermions and spin chains with next-nearest neighbor interactions, Phys. Rev. Res. **3**, 013114 (2021).

[43] L.-Y. Xiao, S.-L. Yu, W. Wang, Z.-J. Yao, and J.-X. Li, Possible singlet and triplet superconductivity on honeycomb lattice, Europhys. Lett. **115**, 27008 (2016).

[44] M. Messer, R. Desbuquois, T. Uehlinger, G. Jotzu, S. Huber, D. Greif, and T. Esslinger, Exploring Competing Density Order in the Ionic Hubbard Model with Ultracold Fermions, Phys. Rev. Lett. **115**, 115303 (2015).

[45] K. Bouadim, N. Paris, F. Hébert, G. G. Batrouni, and R. T. Scalettar, Metallic phase in the two-dimensional ionic Hubbard model, Phys. Rev. B **76**, 085112 (2007).

[46] T. Watanabe and S. Ishihara, Band and Mott insulators and superconductivity in honeycomb-lattice ionic-Hubbard model, J. Phys. Soc. Jpn. **82**, 034704 (2013).

[47] A. Chattopadhyay, S. Bag, H. R. Krishnamurthy, and A. Garg, Phase diagram of the half-filled ionic Hubbard model in the limit of strong correlations, Phys. Rev. B **99**, 155127 (2019).

[48] A. Chattopadhyay, H. R. Krishnamurthy, and A. Garg, Unconventional superconductivity in a strongly correlated band-insulator without doping, SciPost Phys. Core **4**, 009 (2021).

[49] P. Weinberg and M. Bukov, QuSpin: A Python package for dynamics and exact diagonalisation of quantum many body systems. Part II: Bosons, fermions and higher spins, SciPost Phys. **7**, 020 (2019).

[50] J. Hauschild and F. Pollmann, Efficient numerical simulations with tensor networks: Tensor Network Python (TeNPy), SciPost Phys. Lect. Notes **5**, 1 (2018).

[51] P. Thörnig, JURECA: Data centric and booster modules implementing the modular supercomputing architecture at Jülich Supercomputing Centre, J. Large-Scale Res. Facilities **7**, A182 (2021).